Clays and Clay Minerals, Vol. 67, No. 3:228–243, 2019

A NEW KAOLIN DEPOSIT IN WESTERN AFRICA: MINERALOGICAL AND COMPOSITIONAL FEATURES OF KAOLINITE FROM CALUQUEMBE (ANGOLA)

Esperança Tauler[1], Jingyao Xu[1]*, Marc Campeny[1,2], Sandra Amores[1], Joan Carles Melgarejo[1], Salvador Martinez[1], and Antonio O. Gonçalves[3]

[1]Departament de Mineralogia, Petrologia i Geologia Aplicada, Facultat de Ciències de la Terra, Universitat de Barcelona, Barcelona, Spain
[2]Departament de Mineralogia, Museu de Ciències Naturals de Barcelona, Barcelona, Spain
[3]Departamento de Geologia, Universidade Agostinho Neto, Luanda, Angola

Abstract—Large kaolin deposits developed by weathering on Precambrian granitic rocks have been discovered in the Caluquembe area, Huíla province, Angola. To determine accuracy of analysis and to evaluate the kaolinite grade, a full-profile Rietveld refinement by X-ray Powder Diffraction (XRPD) and Thermal Gravimetric Analysis (TGA) was used. Caluquembe kaolin is composed mainly of kaolinite (44–93 wt.%), quartz (0–23 wt.%), and feldspar (4–14 wt.%). The Aparicio-Galán-Ferrell index (AGFI), calculated by XRPD profile refinement, indicates low- and medium-defect kaolinite. Kaolinite particles show a platy habit and they stack together forming 'booklets' or radial aggregates; they also occur as small anhedral particles in a finer-grained mass. Muscovite-kaolinite intergrowths have also been found. Whole-rock chemical analysis included major, trace, and Rare Earth Elements (REE). Chondrite-normalized REE patterns show the same tendency for all samples, with a significant enrichment in Light Rare Earth Elements (LREE). Mineralogical and compositional features of the Caluquembe kaolin indicate that it is a suitable material for the manufacture of structural products, such as bricks, paving stones, and roofing tiles. In addition, the significant REE contents of the Caluquembe kaolin can be considered as a potential future target of mining exploration.

Keywords—AGFI · Angola · Caluquembe · Kaolinite · REE

INTRODUCTION

Kaolinite, $Al_2Si_2O_5(OH)_4$, is a clay mineral, structurally classified as 1:1 layer type, with a crystalline structure comprising tetrahedral and octahedral sheets (Young and Hewat 1988; Moore & Reynolds 1997; Bish 1993). It belongs to the spatial group $C\bar{1}$ with a = 5.154 Å, b = 8.942 Å, c = 7.402 Å, α = 91.69°, ß = 104.61°, and ɣ = 89.92° (Bish 1993).

Kaolinite is classified within the kaolin subgroup, which also includes other minerals such as dickite, nacrite, and a hydrated form of halloysite (Guggenheim et al. 2006). Structural differences between these mineral phases are based on their interlayer shift and the location of the octahedral vacancy in successive layers (Bailey 1980).

Kaolinite is a valuable and versatile industrial mineral with classical applications in the production of bricks, ceramics, paint coatings, paper, and plastic. It also has relatively new applications in catalysis and organic reactivity as well as in the pharmaceutical industry, where it is used in the design of clay-polymer nanocomposites and films (Heckroodt 1991; Murray 1999; Murray 2000; Detellier & Schoonheydt 2014; Phipps 2014; Pruett 2016; Dedzo & Detellier 2016; Nguie et al. 2016; Mansa et al. 2017).

In 2015, world kaolinite production was around 34 million tons (Mt), led mainly by the United States, Germany, Czech Republic, and China, among other countries (Flanagan 2016).

Kaolin deposits are classified as primary, secondary, or tertiary depending on their parent lithology and corresponding alteration processes (Dill 2016). In primary deposits, the parent lithology is a feldspar-rich magmatic rock – mainly granitic or acid volcanic – and the formation of kaolinite is related to feldspar alteration due to hydrothermal fluid circulation and/or the development of weathering processes (Schroeder and Erickson 2014). On the other hand, sedimentary processes generate secondary deposits, composed mainly of detrital clays (Schroeder & Erickson 2014). Tertiary deposits are generated by very low-grade regional metamorphism of argillaceous sediments or sands (Dill 2016).

Angola has significant and large mineral resources. However, for >40 years Angolan independence and civil wars (1961–2002) prevented systematic mining exploration in the country. Nowadays, known mineral resources in Angola include: beryllium, clays, copper, gold, gypsum, iron, lead, lignite, manganese, mica, nickel, phosphates, silver, tungsten, uranium, vanadium, and zinc, among others (Bermúdez-Lugo 2014). However, diamonds are the most economically relevant mineral resource in the country and account for ~5% of worldwide production.

In the case of kaolin, significant deposits have been documented in several regions in Angola (Ekosse 2010). Most are related to weathering of anorthosites from the Kunene anorthositic complex, but systematic studies of these kaolin deposits are still very scarce. The only significant studies were carried out by Gomes et al. (1994) and Savianno et al. (2005)

* E-mail address of corresponding author: jingyao.xu@hotmail.com
DOI: 10.1007/s42860-019-00021-4

on the Mevaiela kaolin deposit, located near the village of Quihita in SE Angola.

In the Caluquembe area (Huíla province, Angola) (Figure 1a), extensive kaolin outcrops associated with weathering of Eburnean granitic rocks were discovered recently. The current study presents the most relevant mineralogical and compositional features of Caluquembe kaolinite. The grade of the kaolinite in the deposit was determined by processing XRPD spectra using full-profile Rietveld refinement and testing the accuracy of the results by TGA. This study also includes major- and trace-elements compositions of the kaolin, with especial interest in the distribution of rare earth elements (REE), in view of the fact that a significant number of REE deposits worldwide are related to weathering of granitic rocks (Nyakairu & Koeberl 2001; Nyakairu et al. 2001; Njoya et al. 2006; Bao & Zhao 2008; Galán et al. 2016; Sanematsu and Watanabe 2016) or from sedimentary rocks (Kadir and Kart 2009; Elliot et al. 2018). The results obtained may be considered as preliminary evaluation guidelines for future mining exploration of kaolin and accessory REEs in the Caluquembe area.

Geological Setting

The Caluquembe area is located in Huíla province (SW Angola), ~180 km NE of Lubango and 570 km SE of Luanda, Angola's capital (Fig. 1a).

Angola's structural framework is generally represented by the Kasai and Congo cratons, which correspond to continental blocks stabilized during the Mesoproterozoic orogeny (Hanson 2003; Jelsma et al. 2011).

The southwestern part of the Congo Craton comprises the Angolan Shield where the presence of widespread Paleoproterozoic crust – dominated by granitoids – has been identified together with a limited amount of Archean crust (De Carvalho et al. 2000; McCourt et al. 2013) (Figure 1a). This basement terrane is intruded by the anorthositic Kunene Complex (Ashwal & Twist 1994; Mayer et al. 2004), a set of Mesoproterozoic red granites, and it is also unconformably overlain by supracrustal sequences.

The Caluquembe region is located in one of the four broad tectonic domains that form the Angolan Shield, known as the Central Eburnean Zone (De Carvalho et al. 2000; Jelsma et al. 2011; McCourt et al. 2013). In this domain, Paleoproterozoic granitoids are the dominant lithologies. However, more recent lithologies such as Eburnean granitoids linked to the Namib thermotectonic event are also found outcropping in this area (De Carvalho et al. 2000). The predominant lithology in the Caluquembe area is the Eburnean Yuabre granites cropping out in association with porphyritic granites (Figure 1b). Hypabyssal rocks such as dolerites, norites, and olivine basalts also occur across the region – related to anorogenic magmatism that occurred in the middle and late Proterozoic and also toward the end of the Cretaceous, during the Wealdenian reactivation of the Angolan platform (~130–100 Ma, Silva and Simões 1980/1981).

Strong erosional processes were developed during the Cenozoic, accompanied by intense weathering under semi-tropical climatic conditions (Marques 1977). The alteration of granitic rocks was related directly to the formation of kaolinite weathering profiles.

SAMPLING AND METHODS

In the present work, 34 samples were studied (Fig. 1b) from extensive weathering profiles developed on granitic rocks in the Caluquembe region (Figure 2). The area studied is ~20 km^2 and sampling was focused mainly on the available outcrops located along river margins.

The morphology and microtextural features of the kaolin samples were examined in polished thin sections using a Nikon Eclipse LV100 POL microscope and an ESEM Quanta 200 FEI, XTE 325/D8395 scanning electron microscope with energy dispersive X-ray spectroscopy (SEM-EDS) at the Scientific and Technological Centers of the University of Barcelona (CCiTUB) (Barcelona, Catalonia, Spain).

Particle size was measured using a Beckman Coulter LS Particle Size Analyzer. To avoid sample flocculation and consequent erroneous measurement of grain-size distribution, ~0.5 g of dry sample was diluted in a dispersing solution of sodium polyphosphate for 15 min in an ultrasonic bath. Before analysis, the resulting solution was agitated for 24 h. This preparation was carried out in the Department of Earth and Ocean Dynamics from the Earth Sciences Faculty of the University of Barcelona (Barcelona, Catalonia, Spain).

Microprobe analyses (EMPA) were performed over selected areas of representative polished thin sections. Analyses were carried out using a JEOL JXA-8230 at the CCiTUB. Analytical conditions were a low voltage of 20 kV (in order to avoid exciting the weaker K and L lines of certain heavy elements which can present spectral interferences), 10 nA beam current, 2 μm beam diameter, and counting time of 10 s per element.

After drying, kaolin samples were crushed, using an agate mortar, for X-ray powder diffraction (XRPD) and thermal analyses (DTA-TGA).

XRPD data were collected using a Panalytical X'Pert PRO MPD X-ray diffractometer (located at the CCiTUB) with monochromatized incident Cu$K\alpha_1$ radiation at 45 kV and 40 mA, equipped with a PS detector with amplitude of 2.113°. Patterns were obtained by scanning randomly oriented powders from 4 to 80°2θ of samples crushed in an agate mortar to a particle size of <40 μm or on oriented mounts. The oriented clay mineral aggregates were prepared by the glass slide method before separating clay minerals from clasts (Moore & Reynolds 1997). Datasets were obtained using a scan time of 50 s at a step size of 0.017°2θ and variable automatic divergence slit. Quantitative mineral phase analyses were obtained by full refinement profile using XRPD. The software used was *TOPAS* V4.2 (2009).

Thermal analyses were carried out by simultaneous DTA-TGA, using a Netzsch instrument (STA 409C model) located at the Department of Mineralogy, Petrology and Applied Geology of the Earth Sciences Faculty of the University of Barcelona (Barcelona, Catalonia, Spain). Analyses were carried out over a temperature range of 25

https://doi.org/10.1007/s42860-019-00021-4 Published online by Cambridge University Press

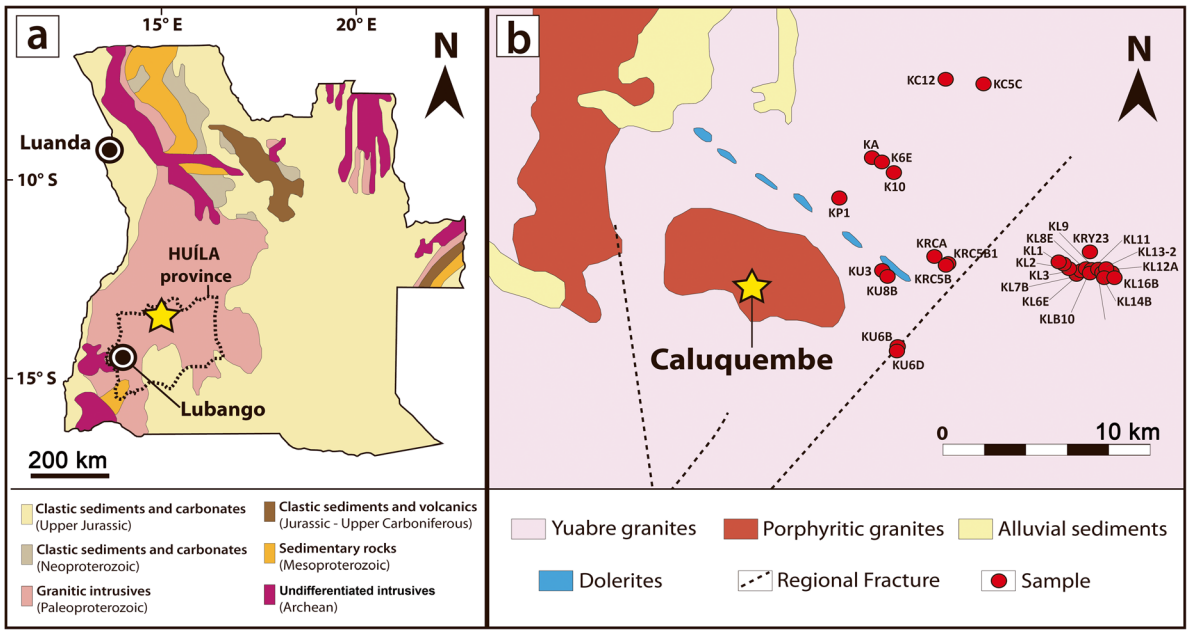

Fig. 1 (a) Simplified geological map of Angola and geographic location of the Caluquembe studied area (yellow star) (modified from Silva 1973); (b) Geological map of the Caluquembe region and location of the studied samples

to 950°C, atmospheric pressure, constant flow rate of 80 mL/min, and at a heating rate of 10°C/min in an Al_2O_3 crucible. The sample amount used was ~80 mg.

Major, minor, and trace elements were determined at ACTLABS Activation Laboratories Ltd., (Ancaster, Ontario, Canada) using the analytical package *4Litho*, using

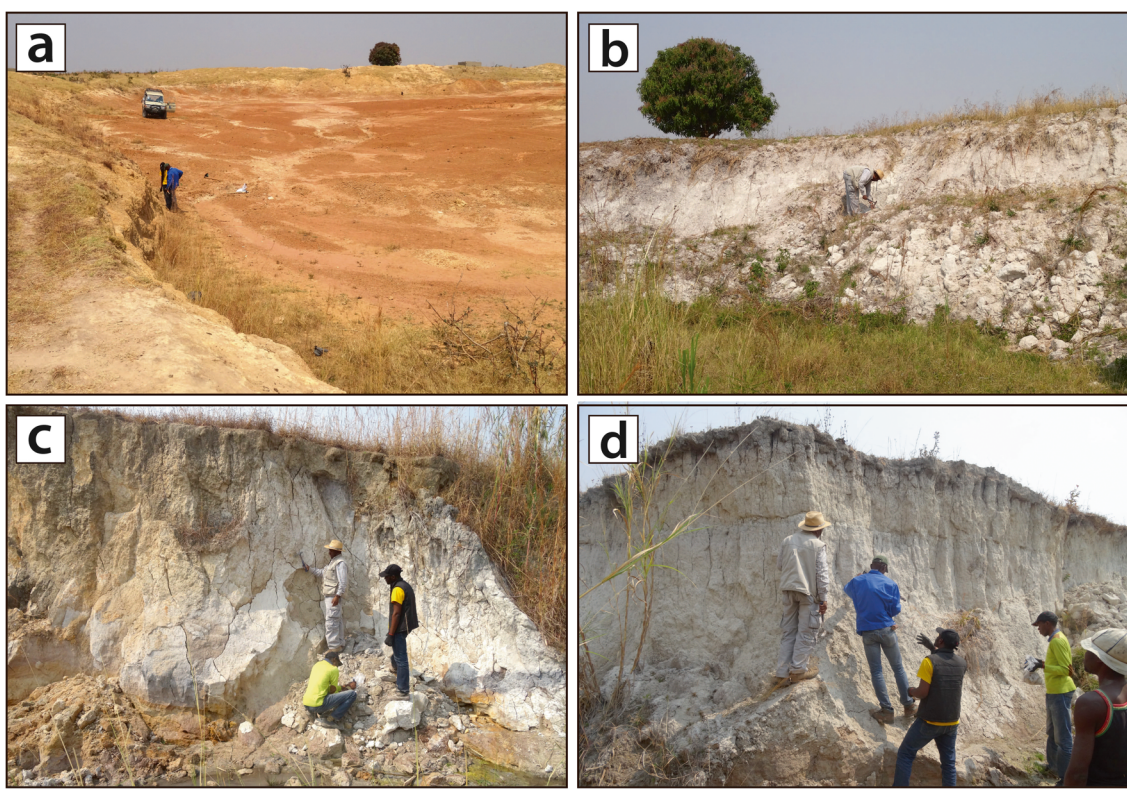

Fig. 2 Views of kaolin outcrops from the Caluquembe area: (a) Plain areas with typical surface alteration due to significant iron contents; (b), (c), and (d) kaolinite outcrops in rivers and creeks of the Caluquembe area

https://doi.org/10.1007/s42860-019-00021-4 Published online by Cambridge University Press

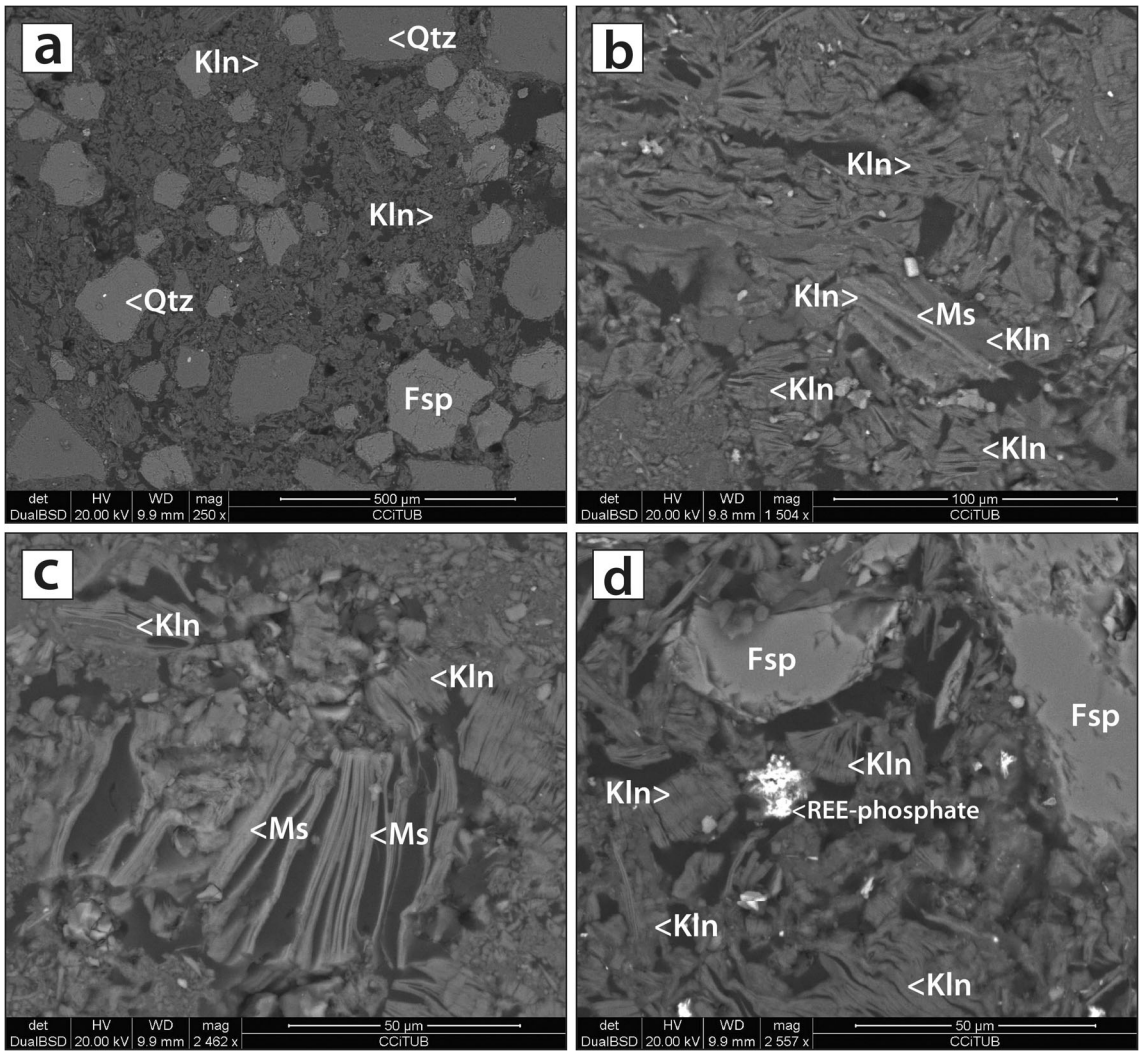

Fig. 3 Backscattered electron images (SEM-BSE) of sample Q-2: (a) quartz (Qtz) and feldspars (Fsp) settled in a finer-grained mass consisting of kaolinite (Kln) and muscovite; (b) Intergrowths of kaolinite (Kln) and muscovite (Ms) scattered in a groundmass comprised of kaolinite; (c) Muscovite (Ms) layers separated along cleavage surfaces; (d) REE phosphate and K-feldspars (Fsp) in a groundmass made up of kaolinite (Kln) forming booklets that are often radial

fusion inductively coupled plasma emission (FUS-ICP) and inductively coupled plasma emission mass spectrometry (ICP-MS) (for details see http://www.actlabs.com). The REE results were normalized with respect to Chondrite (C1, from McDonough & Sun 1995) and Upper Continental Crust (UCC, Rudnick & Gao 2003).

RESULTS

Kaolin Petrography

Kaolin samples are made up of soft powder with white to gray, pale yellow, and pale brown colors, containing some consolidated fragments.

Particle-size distribution of Caluquembe kaolin shows that that silt fraction is predominant whereas clay and sand fractions are less abundant. Therefore, 4.9–8.8 vol.% of kaolin particles are <2 µm in size; 54.1–75.1 vol.% are between 2 and 63 µm; 12.6–17.9 vol.% are between 63 and 125 µm; and 3.3–12 vol.% are between 125 and 250 µm.

Quartz, microcline, and plagioclase (albite) are set in a finer-grained mass (groundmass) composed of muscovite and kaolinite (Fig. 3a). Quartz occurs as irregular fragments 500 µm in size with typical angular borders. Anhedral grains of microcline are up to 200 µm in diameter and are altered commonly to cryptocrystalline kaolinite. Plagioclase has a grain size of <100 µm and is also altered to sericite. SEM-BSE images show that in the finer-grained mass, muscovite occurs as tabular crystals (50 µm long) while particles of kaolinite often show a platy habit and are stacked together forming `booklets' or radial aggregates, both phases can also be found as very fine anhedral particles (Fig. 3b). Some particles of muscovite are separated by cleavage (Fig. 3c). Kaolinite

https://doi.org/10.1007/s42860-019-00021-4 Published online by Cambridge University Press

Table 1 Mineral content (wt.%) calculated by XRPD profile refinement with Topas V4.2

Sample	Full profile refinement XRPD (wt. %)						TGA		
	Kaolinite	Muscovite	Quartz	Plagioclase	Microcline	Hematite	Tm (°C)	Mass loss (wt.%)	Kaolinite (wt. %)
KA	87	8.6	0.3	2	2.1	0.02	550.3	12.0	85.9
K6E	67.2	10.7	13.1	5.9	3	0.06	531.0	8.6	61.1
K10	64.3	17	10.1	5.3	3.2	0.05	529.3	8.6	61.1
KP1	70.8	8.5	2.8	1.97	11.9	1.6	539.1	9.7	68.9
KC12	50.4	21.3	23.5	3.8	0.9	0.07	518.7	6.7	47.9
KC5 C	51.2	27.3	11.5	7.4	2.6	0.04	530.4	7.9	56.2
KU3	79.2	1.1	14.8	2.9	1.4	0.58	526.6	10.9	77.6
KU6B	71.5	3.9	7.7	1.8	15.1	0	531.4	10.9	78.0
KU6D	58.9	5.5	10.5	3.6	21.5	0.04	520.0	6.2	44.3
KU8B	54.6	24.6	8.8	2.1	9.8	0.07	530.1	7.5	53.4
KRC3B	63.3	21.4	2.9	0.3	12.1	0.03	542.4	9.9	70.4
KRC5B	62.8	23.9	3.5	3.9	5.9	0.04	540.8	9.4	67.2
KRC5B1	64.1	20.8	4	4.6	6.5	0.03	541.0	9.0	64.3
KRY23	76.7	9.9	7.7	0.9	4.8	0.03	532.3	9.2	65.5
KRCA	77.3	8.4	5.7	4.5	4.1	0.04	546.0	11.2	80.0
KK14C	60.6	29.2	4.3	0.3	5.1	0.5	528.3	7.9	56.2
KKL13B	71.3	17.2	5.3	1.7	4.4	0.06	534.2	9.4	67.4
KKL17B	76.2	11.5	4.2	4	4.1	0.04	541.8	10.4	74.4
KL9	62.4	12.4	15.1	4.3	5.7	0.11	525.4	7.2	51.5
KL11	67.6	14.9	10.2	1.7	5.5	0.06	537.6	8.3	59.2
KL12A	76.2	11.2	4.8	4.7	3	0.06	536.0	10.0	71.0
KL13-2	84.2	2.9	0	5.7	6.7	0.5	540.3	10.5	74.8
KL14B	60.6	26	5.1	1.2	7.1	0.02	541.6	7.8	56.0
KL16B	72.4	15.4	5.3	2.6	4.1	0.2	537.2	9.0	64.0
L-1	86.6	3.9	1.9	6.3	1.2	0.1	527.9	13.0	92.9
L-2	79	7.3	6.9	3.2	3.6	0.01	518.4	10.1	72.4

Temperature of dehydration (Tm) of kaolinite, mass loss and kaolinite content (wt.%) calculated by TGA.

is also found as muscovite-kaolinite intergrowths (up to 50 μm long), which was distinguished using EDS microanalysis (Fig. 3b). Phosphate enriched in LREE, probably monazite-(Ce), is also found as an accessory mineral phase (Fig. 3d).

X-ray Powder Diffraction (XRPD)

The quantitative analysis of 26 whole-rock random powders (XRPD) shows that samples are composed mainly of kaolinite (50.4–87.0 wt.%), quartz (0–23.5 wt.%), albite (0.3–7.4 wt.%), microcline (1.2–21.5 wt.%), and muscovite (1.1–29.2 wt.%) (Table 1). Scarce hematite (<1 wt.%) is also found in some samples; sample KP1, which contains a significant amount of accessory minerals, contains 1.6 wt.% of hematite and 2.4 wt.% of calcite. The shallower samples (KA, KU3, KU6B, KKL17B, KL13-2, L-1, and L-2) are richer in kaolinite than samples obtained from the base of the profiles. For instance, samples KU6B (shallow) and KU6D (deep) from the same outcrop contain 71.5 wt.% and 58.9 wt.% of kaolinite, respectively (Table 1).

XRPD profile refinement of sample KL13-2 revealed a significant percentage of kaolinite (84.2 wt.%), <1 wt.% of quartz, and a very small muscovite content (2.9 wt.%) (Figure 4a). Sample KC12 has more quartz (23.5 wt.%) and muscovite (21.3 wt.%), and less kaolinite (50.4 wt.%). A negative correlation ($R^2 = 0.67$) between the contents of kaolinite and muscovite plus K-feldspar is evident in the samples analyzed (Figure 5).

The average crystallite size for kaolinite is 15–35 nm, calculated from the profile refinement by XRPD.

Five samples containing illite and three samples containing smectite were identified (Table 2). The three smectite-bearing samples (KL6E, KL8E*, and KLB10) are located in the deepest part of the outcrop, containing a low kaolinite grade (Table 2). Illite-bearing samples KK13 and KK11A also contain goethite: 12.9 wt.% and 22.9 wt.%, respectively.

The XRPD patterns of three samples show the d_{001} of illite, muscovite, smectite, and kaolinite in the region of 4–15°2θ (Fig. 6). The d_{002} band for illite at 10.03 Å was broader and less intense than that for muscovite at d_{002} = 9.97 Å. A

https://doi.org/10.1007/s42860-019-00021-4 Published online by Cambridge University Press

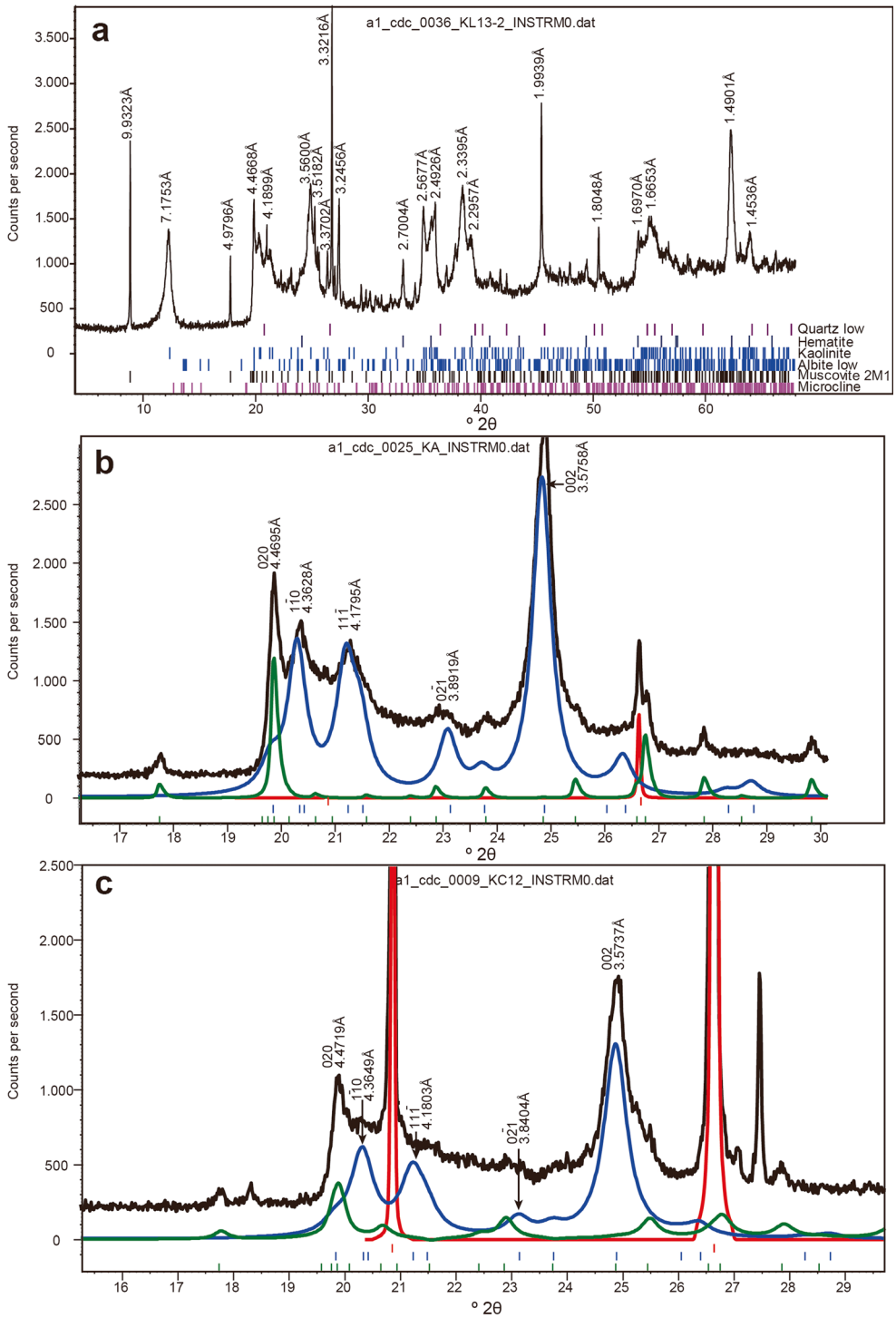

Fig. 4 (a) XRPD profile refinement (by *Topas* V4.2 software) of sample KL13-2 with the spacing of the more intense reflections. The calculated Bragg positions of mineral phases are shown at the bottom, Rwp = 8.7 (agreement with weighted profile factor in the Rietveld method); (b) XRPD profile refinement of sample KA in the region 17–30°2θ. The black line corresponds to the experimental XRD profile of this sample. The blue line corresponds to the calculated XRD profile of kaolinite. The red and green lines correspond to calculated XRD profiles of quartz and muscovite, respectively, Rwp = 11.3; (c) XRPD profile refinement of sample KC-12 in the region 16–29°2θ. The black line corresponds to the experimental XRD profile of this sample. The blue line corresponds to the calculated XRD profile of kaolinite. The red and green lines correspond to calculated XRD profiles of quartz and muscovite, respectively, Rwp=14.1.

https://doi.org/10.1007/s42860-019-00021-4 Published online by Cambridge University Press

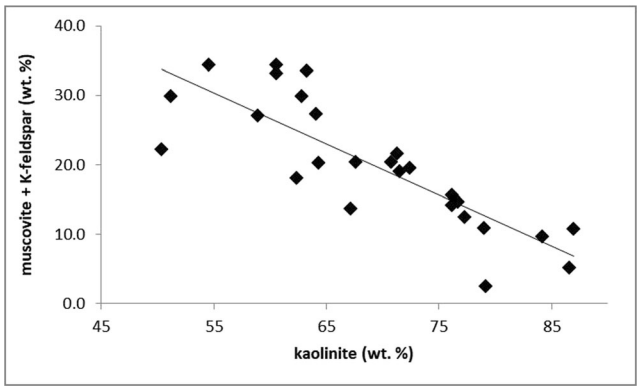

Fig. 5 Relation between muscovite+K-feldspar vs. kaolinite (wt. %) calculated by XRPD profile refinement with Topas V4.2

broad and low-intensity maximum for smectite was noted at d_{001} = 14.9 Å. The d_{001} of kaolinite at 7.14 Å shows no appreciable differences in the XRPD profile of these samples and is narrow and intense.

Kaolinite was distinguished in the XRD patterns of oriented mounts; the the d_{001} reflections disappeared after heating to 550°C. No variations were detected after ethylene glycol treatment. In contrast, the XRD patterns of oriented mounts of samples with smectite had significant changes. The peak at d_{001} = 14.9 Å changed to 17 Å when solvated in ethylene glycol, and changed to 10 Å when the sample was heated to 550°C. Samples with illite showed only a slight expansion of the broad reflection at d_{002} = 10.03 Å when solvated in ethylene glycol, indicating a small proportion of expanded clay (Thorez 1975; Moore & Reynolds 1997).

The physical properties of kaolin, such as whiteness, abrasiveness, particle size, shape and distribution, viscosity, and rheology vary depending on the genetic conditions of the deposits. The kaolinite crystallinity index (KCI) may be significant for the calculation of the degree of crystal perfection in kaolinite, which is an essential parameter when evaluating kaolinite quality for industrial applications, in addition to the plasticity correlation. In the XRPD pattern, reflections 020, $1\bar{1}0$ and $11\bar{1}$ were detected in the 20–23°2θ region. These reflections are sensitive to random and interlayer displacements and enable the various KCI to be calculated (HI from Hinckley 1963; IK from Stoch 1974; AGFI from Aparicio et al. 2006). The Hinckley crystallinity index (HI, Hinckley 1963) is one of the most widely used indices. Normal values range from <0.5 (disordered) to 1.5 (ordered). The calculated HI index in the 20–23°2θ region was 1.06 in sample KA, 1.05 in sample KC12, and 1.09 in sample KL12A. The HI of Caluquembe kaolin is generally higher than reported in other kaolin deposits worldwide such as the sedimentary kaolin from Georgia (USA) with 0.56 HI or the kaolin from Montecastelo (Spain) with an HI of 1.00 (Aparicio et al. 2006). The IK index or Stoch index (Stoch 1974) is measured in the same zone as for HI, and the normal values range from >1.0 (disordered) to <0.7 (ordered). The calculated IK index in the 20–23°2θ region is 1.04 (disordered) in sample KL12A.

According to Aparicio and Galán (1999), the KCI can be determined only as an approximate value. Kaolinite

Table 2 Mineral content (wt.%) calculated by XRPD profile refinement with Topas V4.2 in samples with smectite and illite

Sample	Full profile refinement XRPD (wt.%)								TGA		
	Kaolinite	Muscovite	Illite	Smectite	Quartz	Plagioclase	Microcline	Hematite	Tm (°C)	Mass loss (wt.%)	Kaolinite (wt.%)
KK8	54	12	15		9	4	6	0	520.1	7.7	54.8
KK11A	57.6		8.1		5.7	2.1	3.6	0.0	531.6	7.1	50.9
KK13	59.3		7.4		9.6	2.8	8.0	0.2	528.3	7.0	50.0
KL6E	29.4	30.6		16.7	5.5	11.5	6.3	0.0	525.9	5.8	41.2
KL7B	56.5	9.9	18.4		3.8	4.8	6.5	0.0	535.0	8.8	63.1
KL8E*	34.8	23.8		15.8	4.8	6.0	14.5	0.4	537.7	7.6	54.6
KLB10	47.4	24.0		10.1	5.5	4.0	9.0	0.1	530.8	8.3	59.5
L-3	68.6	2.7	22.1		3.9	2.0	0.6	0.0	521.9	7.9	56.2

Temperature of dehydration (Tm) of kaolinite, mass loss and kaolinite content (wt.%) calculated by TGA.

https://doi.org/10.1007/s42860-019-00021-4 Published online by Cambridge University Press

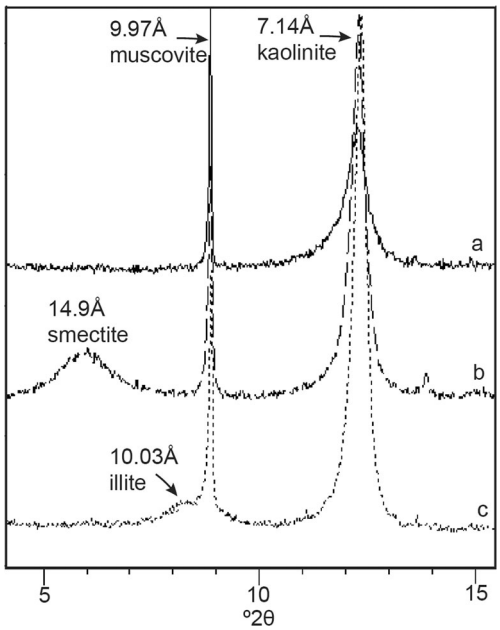

Fig. 6 XRPD of samples in the region from 4° to 15° 2θ: (a) KL13-2, muscovite and kaolinite; (b) KL6E muscovite, kaolinite, and smectite; (c) KK8, muscovite, kaolinite, and illite

maxima by XRPD are close to the muscovite and quartz maxima in the 20–23°2θ region. Aparicio et al. (2006) presented the new AGFI (Aparicio-Galán-Ferrell Index) based on additional processing to decompose overlapping peaks detected in the region of interest with the *MacDiff* software (Petschick 2004).

Peak intensities of 020, $1\bar{1}0$ and $11\bar{1}$ in kaolinite have been determined through full-profile refinement by XRPD using the software *Topas* V4.2 in samples from Caluquembe. Sample KA has <1 wt.% of quartz and 9 wt.% of muscovite, and an AGFI of 1.06 (Fig. 4b). Sample KC12 has quartz (24 wt.%) and muscovite (21 wt.%), with an AGFI of 1.35 (Fig. 4c). Sample KL12A has 5 wt.% of quartz and 20 wt.% of muscovite and an AGFI of 1.19. According to Aparicio et al. (2006), these samples can be classified as low- and medium-defect kaolinite. Similar data were obtained by Aparicio et al. (2006) in kaolinite from Mevaiela (Angola). In this case, the AGFI is 1.35 in kaolinite containing 20 wt.% quartz, which suggests that AGFI is more accurate at determining the crystallinity of the sample and is also related to the kaolinite content.

Differential Thermal and Thermogravimetric Analysis (DTA-TGA)

The DTA curve (Figure 7) shows only an endothermic peak only in dry-air conditions at 540.3°C in sample KL132, confirming the dehydration of kaolinite (MacKenzie 1957; Liu et al. 2015). Samples had a mass loss of between 6.2 and 13.0 wt.% up to 650°C in the TGA curve. Samples with greater kaolinite contents showed a more significant mass loss. The amount of kaolinite calculated by mass loss was between 44.3 and 92.9 wt.% (Table 1).

Correlation Between TGA and XRPD

Thermal analyses were carried out to check the quantitative results of mineral phases calculated by XRPD using the correlation between the calculated wt.% of kaolinite in the profile refinement by XRPD and the calculated wt.% of kaolinite in TGA (Fig. 8). Samples containing more kaolinite also have greater mass loss indicating a positive correlation (R^2 = 0.75). The proposed model demonstrates an adequate accuracy for the quantification of kaolinite and shows that material sampled closer to the surface is richer in kaolinite than samples from the deeper part of the profile. The quantitative results of samples containing illite and smectite give less accurate values because the thermal

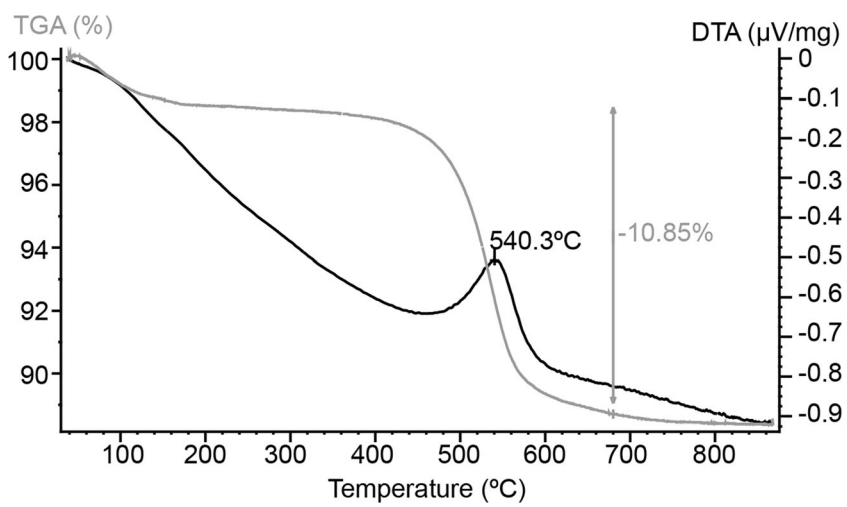

Fig. 7 DTA-TGA curves of kaolin from Calumquembe of sample KL13-2. DTA (black line) - TGA (gray line)

https://doi.org/10.1007/s42860-019-00021-4 Published online by Cambridge University Press

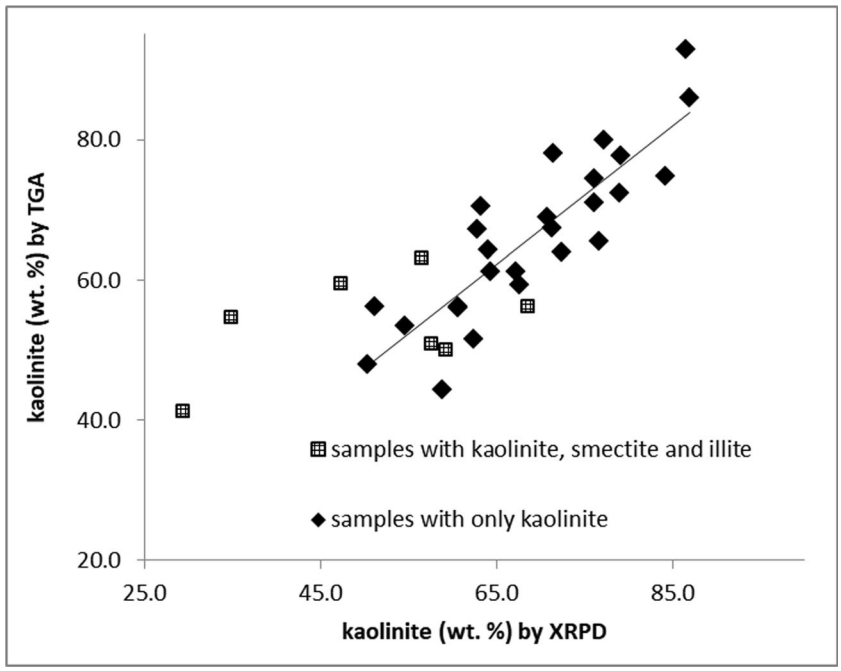

Fig. 8 Kaolinite content (wt.%) calculated by XRPD with Topas V4.2 vs. kaolinite content (wt. %) calculated by mass loss in TGA

characteristics of kaolinite are influenced by the presence of smectite and illite.

Kaolin Geochemistry

The average chemical composition of kaolinite determined by EMPA is: 46.28 SiO_2, 36.31 Al_2O_3, 0.58 MgO, 0.03 Na_2O, 0.10 TiO_2, 0.85 Fe_2O_3, 0.03 MnO, 0.04 BaO, 0.07 CaO, 0.05 K_2O wt.%. The average structural formula based on 14 oxygens is as follows $(Al_{3.77}Fe^{3+}_{0.05}Mg_{0.06})_{3.9}Si_{4.0}O_{10}(OH)_8$.

Major- and trace-element, REE concentrations were obtained from six representative samples from the Caluquembe area (Tables 3, 4, and 5). Two kaolin samples from Uganda (Nyakairu & Koeberl 2001), one from Cameroon (Njoya et al. 2006) and one from the Sa Bandeira granite in Huambo (Angola) are also shown for comparison in Tables 3 and 4. Sa Bandeira granite has a very similar composition to the granites which crop out in the Caluquembe area (Montenegro de Andrade 1954).

Major elements generally show a different trend in the altered sample compared to the parent rock (Table 3). The SiO_2 trend of Caluquembe kaolin is decreasing and the Al_2O_3 trend is increasing compared to the granite from Sa Bandeira. SiO_2 is high for all samples ranging between 45.35 and 63.24 wt.%. Al_2O_3 contents lie between 21.89 and 32.24 wt.%. Fe_2O_3 is between 1.36 and 4.25 wt.%. K_2O is between 1.16 and 4.03 wt.%. TiO_2 is between 0.49 and 0.86 wt.%. Other remaining oxides (Mn, Mg, Ca, Na) are present only as traces (<0.2 wt.%). Loss on ignition (LOI) values are between 7.80 and 13.69 wt.%.

The most abundant trace elements are: Zr from 162 (sample L1) to 430 (sample K6E) ppm; Ba from 222 (sample K6E) to 1090 (sample KL13-2) ppm; Rb from 54 (sample KL13-2) to 206 (sample KLB 10) ppm. Other trace elements such as Sc, V, Cr, Co, Ni, Cu, Zn, Ga, Sr, Y, Nb, Hf, Pb, Th, and U are usually <100 ppm. As, Nb, Ag, In, Sn, Sb, Cs, Ta, W, and Bi are <5 ppm (Table 4).

The REE contents in kaolin samples (Table 5) vary from 130 ppm (sample L1) to 564 (sample KL13-2) ppm. REY (REE+Y) range between 142 ppm and 624 ppm. LREE (La, Ce, Pr, Nd, Sm, Eu) range from 524 to 122 ppm while HREE (Heavy Rare Earth Elements) (Gd, Tb, Dy, Ho, Er, Tm, Yb, Lu) range from 40 to 8 ppm (Table 4). The C1 chondrite-normalized REE plots (Figure 9a) (McDonough & Sun 1995) are roughly parallel and characterized by negative slopes as a result of enrichment in the LREE relative to HREE. The normalization via upper Continental Crust (UCC, Rudnick & Gao 2003) is presented in Figure 9b. In general, Caluquembe samples present flat REE patterns. They also have a negative Sc anomaly as reported in heavy and grit mineral fractions from Georgia kaolin. Only sample L-1 from Caluquembe has a different behavior with a Sc enrichment of the light fraction from the Jeffersonville and Buffalo Creek Members in Georgia, USA (Elliot et al. 2018).

DISCUSSION

Classification of the Caluquembe Deposit

Considering the small amount of geological information available about this area, it is necessary to establish a formal classification of the Caluquembe kaolin deposit using the

https://doi.org/10.1007/s42860-019-00021-4 Published online by Cambridge University Press

Table 3 Major element compositions of kaolin samples (wt.%) and CIA calculated from molar proportions of Al_2O_3, Na_2O, K_2O, and CaO from: Caluquembe, Angola; sample BW-1 from Buwambo and MG-1 from Migade, Uganda (Nyakairu et al. 2001); sample MY03 from Mayouom, Cameroon (Njoya et al. 2006); granite from Sa Bandeira, Angola (Montenegro de Andrade 1954)

Major elements	Caluquembe Angola	Caluquembe Angola	Caluquembe Angola	Caluquembe Angola	Caluquembe Angola	Caluquembe Angola	Buwambo Uganda	Migade Uganda	Mayouom Cameroon	Huambo Angola
wt.%	KU6B	KU6D	KL13-2	K 6E	KLB 10	L1	BW-1	MG-1	sand-p MY03	Sa Bandeira
SiO_2	53.10	63.24	45.35	56.08	51.57	48.76	49.98	49.90	46.61	72.21
Al_2O_3	27.72	21.89	31.79	26.60	27.07	32.24	35.97	35.62	33.29	15.02
TiO_2	0.57	0.49	0.86	0.79	0.69	0.62	0.02	0.05	3.96	0.40
Fe_2O_3(T)	3.58	1.54	4.15	1.36	4.25	2.75	0.34	0.54	1.46	0.29
MnO	0.02	0.01	0.18	0.01	0.02	0.02	0.05	0.04	< dl	0.06
MgO	0.52	0.31	0.50	0.17	0.80	0.52	0.33	0.34	< dl	0.80
CaO	0.13	0.15	0.18	0.09	0.08	0.06	<0.010	<0.01	< dl	2.37
Na_2O	0.07	0.14	0.03	0.01	0.04	0.01	0.03	0.04	< dl	3.23
K_2O	3.55	4.03	2.02	1.16	3.63	1.65	0.99	0.78	0.94	3.86
P_2O_5	0.04	0.03	0.01	0.08	0.03	0.01	0.06	0.11	0.40	0.08
LOI	10.55	7.80	13.69	12.71	10.98	12.48	12.61	12.85	13.97	1.00
Total	99.84	99.64	98.74	99.07	99.17	99.13	100.35	100.23	99.87	100.50
CIA	87	82	93	95	87	92	97	97	97	52

Table 4 Trace elements (ppm) of samples from Caluquembe, Angola; sample BW-1 from Buwambo and MG-1 from Migade, Uganda (Nyakairu et al. 2001); sample MY03 from Mayouom, Cameroon (Njoya et al. 2006)

	Caluquembe Angola	Caluquembe Angola	Caluquembe Angola	Caluquembe Angola	Caluquembe Angola	Caluquembe Angola	Buwambo Uganda	Migade Uganda	Mayouom Cameroon
ppm	KU6B	KU6D	KL13-2	K 6E	KLB 10	L1	BW-1	MG-1	sand-p MY03
Be	4	3	3	3	3	4	n.d.	n.d.	<dl
V	101	69	51	54	77	74	<15	<15	718
Cr	< 20	< 20	< 20	30	< 20	20	4.47	10.9	294
Co	6	5	10	8	7	7	1.3	1.75	1.8
Ni	< 20	< 20	< 20	< 20	< 20	< 20	19	24	5.4
Cu	10	< 10	50	20	50	10	52	105	n.d.
Zn	60	50	50	50	90	60	16	24	43.2
Ga	36	29	42	31	34	26	n.d.	n.d.	38
Ge	2	2	2	2	2	2	n.d.	n.d.	1.77
As	< 5	< 5	5	< 5	< 5	< 5	0.12	0.23	n.d.
Rb	167	155	54	113	206	130	58.3	58	17.3
Sr	40	41	65	20	44	22	39.1	65.9	383
Zr	368	281	337	430	278	162	142	139	489
Nb	18	15	22	24	14	17	6	6	57.9
Mo	< 2	< 2	2	< 2	< 2	< 2	n.d.	n.d.	4.08
Ag	1.3	1	1.3	1.5	1	< 0.5	n.d.	n.d.	n.d.
In	< 0.2	< 0.2	< 0.2	< 0.2	< 0.2	< 0.2	n.d.	n.d.	0.18
Sn	3	2	4	4	5	3	n.d.	n.d.	3.51
Sb	< 0.5	< 0.5	< 0.5	< 0.5	< 0.5	< 0.5	n.d.	n.d.	n.d.
Cs	3.3	3	< 0.5	5.9	2.4	3.9	2.27	3.61	1.01
Ba	595	683	1090	222	871	307	63.2	114	644
Bi	< 0.4	< 0.4	1.5	< 0.4	< 0.4	0.6	n.d.	n.d.	n.d.
Hf	9.8	7.5	8.7	10.7	6.9	4.9	0.66	0.86	11.2
Ta	1.8	1.7	2.3	3.1	1.7	1.6	0.34	0.38	4.44
W	5	3	13	6	6	4	n.d.	n.d.	0.8
Tl	0.8	0.7	0.5	0.6	0.9	0.5	n.d.	n.d.	n.d.
Pb	36	36	40	38	22	26	n.d.	n.d.	9.62
Th	25.1	20.1	48.6	31.7	16.9	17.9	1.66	1.25	6.86
U	7.1	6	5.6	17.2	16.1	5.9	0.84	1	1.75

n.d. = not detected, <dl = below detection limit.

mineralogical and compositional data obtained in the present work.

Kaolinite from Caluquembe is generally found as a finer-grained mass of particles, though muscovite-kaolinite intergrowths are also reported. Considering the results of the granulometric curve, particle-size distribution of the Caluquembe kaolin shows small amounts of the <4 μm fraction (8.7 to 13.8 vol.%), which correspond to the kaolinite that originated by alteration of potassium feldspar, while muscovite-kaolinite intergrowths may correspond to the <63 μm fraction (74.0 to 83.9 vol.%).

The Chemical Index of Alteration (CIA) is also a very suitable parameter to determine the weathering level of feldspars and the corresponding formation of kaolin by this process (Nesbitt & Young 1984). CIA is expressed from 0 to 100 and it is calculated using the molar proportions of oxides of the main compositional elements of kaolin: Al, Na, K, and Ca [$CIA = Al_2O_3/(Al_2O_3+Na_2O+K_2O+CaO)\cdot 100$]. The CIA parameters of the Caluquembe kaolin have indexes from 82 to 95 (Table 3), which are significant and indicate an elevated level of feldspar alteration. In addition, it is possible to distinguish changes in the CIA parameter between kaolin samples obtained from different levels of the same outcrop. For instance, in sample KU6B (upper level) and sample KU6D (lower level), the CIA parameter is 87 and 82, respectively, indicating a significant increase in weathering in the upper levels which is also directly related to the kaolinite content: 71.5 and 58.9 wt.%, respectively.

During intense weathering, potassium feldspar and plagioclase were destabilized and transformed to kaolinite, while sericite and muscovite were also transformed to kaolinite especially in the upper levels of the profile (Galán 2006). This

https://doi.org/10.1007/s42860-019-00021-4 Published online by Cambridge University Press

Table 5 REE (ppm) of samples from Caluquembe, Angola; sample BW-1 from Buwambo and MG-1 from Migade, Uganda (Nyakairu et al. 2001); sample MY03 from Mayouom, Cameroon (Njoya et al. 2006); C1 chondrite (McDonough & Sun 1995) and UCC (Rudnick & Gao 2003) used for the normalization

	Angola	Angola	Angola	Angola	Angola	Angola	Uganda	Uganda	Cameroon		
ppm	KU6B	KU6D	KL13-2	K 6E	KLB 10	L1	BW-1	MG-1	sand-p MY03	UCC	C1Ch.
La	57.5	53.1	138	91.3	44.6	27.4	101	215	120	31	0.237
Ce	92.2	114	232	156	67	67	37.5	143	243	63	0.613
Pr	14	12.9	29.5	19.4	9.59	5.23	n.d.	n.d.	27.3	7.1	0.0928
Nd	50.8	46.2	103	67.5	32.6	18.4	51.5	159	96.5	27	0.457
Sm	8.9	8.5	17.5	12.1	5.3	3	9.69	15.8	20.3	4.7	0.148
Eu	1.74	1.69	3.8	2.37	1.1	0.65	2.16	2.25	5	1	0.0563
Gd	6	5.6	11.8	8.4	3.5	2.1	5.51	4.61	17.4	4	0.199
Tb	0.8	0.8	1.7	1.3	0.5	0.4	0.9	0.71	2.34	0.7	0.0361
Dy	4.7	4.1	10.4	7.4	2.8	2	n.d.	n.d.	12.7	3.9	0.246
Ho	0.9	0.7	2	1.4	0.5	0.4	n.d.	n.d.	2.09	0.83	0.0546
Er	2.6	2.2	6	3.9	1.7	1.2	n.d.	n.d.	4.86	2.3	0.16
Tm	0.41	0.32	0.9	0.59	0.29	0.19	0.26	0.29	0.7	0.3	0.0247
Yb	2.8	2.2	6	4.1	2.2	1.4	1.21	1.03	4.1	2	0.161
Lu	0.45	0.35	0.9	0.64	0.36	0.21	0.14	0.1	0.6	0.31	0.0246
Sc	14	11	14	15	12	14	1.2	1.89	0	14	5.92
Y	26	20	60	39	16	12	10	8	48.3	21	0.026
∑REE	243.8	252.66	563.5	376.4	172.04	129.58	209.87	541.79	556.89		
∑LREE	225.14	236.39	523.8	348.67	160.19	121.68	201.85	535.05	512.1		
∑HREE	18.66	16.27	39.7	27.73	11.85	7.9	8.02	6.74	44.79		
LREE/HREE	12.07	14.53	13.19	12.57	13.52	15.40	25.17	79.38	11.43		
La/Th	2.29	2.64	2.84	2.88	2.64	1.53	60.84	172.00	17.49		
Y/HREE	1.39	1.23	1.51	1.41	1.35	1.52	1.25	1.19	1.08		

n.d. = not detected.

explains why the kaolinite content decreases towards the deeper parts of the weathering profile as reported in the samples from the Caluquembe area.

The ratios of La/Th and Y/HREE may also be useful parameters to determine kaolin provenance. In the case of Caluquembe kaolin, the La/Th ratio is 2.7, which is similar to values reported in upper continental crust (2.8 ± 0.2), indicating a felsic source for kaolin (Taylor & McLennan 1995). Likewise, Y/HREE ranges from 1.2 to 1.5, indicating a similar process during kaolinization.

Eu anomalies associated with more evolved continental crust are found, for instance, in clay-rich sediments from central Uganda (Nyakairu & Koeberl 2001), in samples from weathered granitic rocks of south China (Bao & Zhao 2008), in samples from Sögüt in northwestern Turkey (Kadir & Kart 2009) and in samples from residual kaolin derived from granitic rock in SE Germany (Dill 2016). This Eu anomaly is not found in samples from Caluquembe (Figure 9a, Table 5).

The compositional and mineralogical features of the kaolin deposits from the Caluquembe area offer strong evidence indicating that they originated from the weathering of precursor granitic rocks. Therefore, kaolin deposits from Caluquembe should be classified as primary kaolin deposits (Dill 2016).

Economic Interest

The potential extent of kaolin outcrops in Caluquembe is estimated to be ~20 km^2, with a significant thickness ranging from 5 to 10 m (Figure 2). At present, a further evaluation is being carried out in the area to obtain a more accurate assessment of the extent and thickness of the kaolin deposits. However, the preliminary estimate is that the potential inferred reserves of kaolin in the Caluquembe area are estimated at ~500,000,000 m^3. Although this calculation is approximate and more accurate studies are necessary, this preliminary volume suggests that Caluquembe is a medium-sized kaolin deposit, bigger than other deposits from western Africa such as that at Makoro, Botswana (Ekosse 2000).

The Al_2O_3 contents of kaolin are directly related to the kaolinite percentage and are therefore considered to be a significant parameter for determining kaolin quality. Caluquembe Al_2O_3 contents (21.9 to 32.2 wt.%) and SiO_2/Al_2O_3 ratio (1.28) are similar to those reported for kaolin from the Zhanjiang, Longyan, and Dazhou deposits (Guangdong Province, China; Wilson et al. 1997), and slightly higher than the theoretical value for kaolinite (1.16). However, the Fe_2O_3 contents of Caluquembe kaolin are quite significant (1.4 to 4.3 wt.%) and likely to affect the marketing potential of the

https://doi.org/10.1007/s42860-019-00021-4 Published online by Cambridge University Press

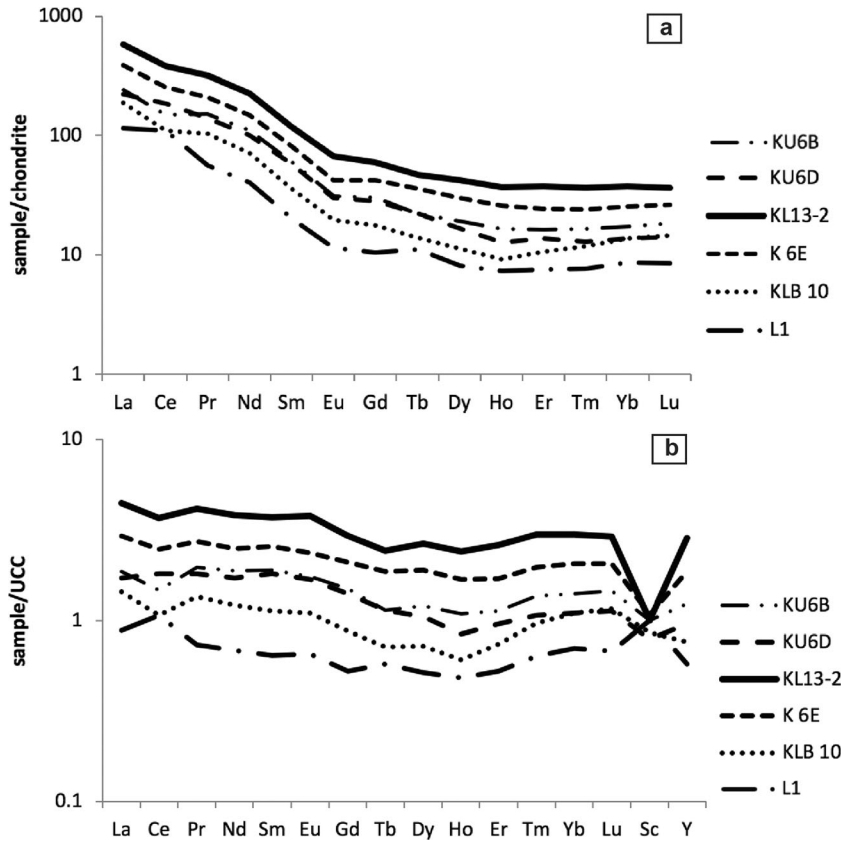

Fig. 9 The enrichment/depletions of REE of Caluquembe kaolin samples: (a) Results normalized to C1 chondrite (McDonough and Sun 1995); (b) Results normalized to UCC (Rudnick and Gao 2003)

Caluquembe kaolin (Saikia et al. 2003; López-Galindo et al. 2007).

The mineralogical and chemical compositions of kaolin from Caluquembe are similar to other African kaolins (Table 6). In addition, the kaolinite grade is slightly lower or similar to those found in Koutaba and Mayouom in Cameroon (Njoya et al. 2006; Nkalih Mefire et al. 2015), central Uganda (Nyakairu et al. 2001), Makoro in Botswana (Ekosse 2000), and Grahamstown in South Africa (Heckroodt 1991). The mineralogical composition of three classical kaolin deposits developed from precursor granites is presented for comparison in Table 6: Guandong (China), Otovice (Czech Republic), and Cornwall (UK). All have greater kaolinite contents than the Caluquembe deposit.

Given the main features of Caluquembe kaolin, its main uses should be in the fabrication of bricks, paving slabs, roofing tiles, and the ceramics industry (Heckroodt 1991; Gomes et al. 1994; Ekosse 2000; Nyakairu et al. 2001; Savianno et al. 2005; Njoya et al. 2006; Ekosse 2010; Nkalih Mefire et al. 2015).

In addition, kaolin deposits have recently been considered non-conventional sources of critical metals such as REE (Aagaard 1974; Laufer et al. 1984; Xiao et al. 2016; Sanematsu and Watanabe 2016; Elliot et al. 2018). Values of ∑REE (La, Ce, Pr, Nd, Sm, Eu, Gd, Tb, Dy, Ho, Er, Tm, Yb, Lu) in Caluquembe are highly erratic, 129.58 ppm to 563.5 ppm (Table 4), and do not correlate with SiO_2, Fe_2O_3, CaO, P_2O_5, or MnO. Samples are more enriched in LREE (Table 5) and the ratio LREE/HREE is homogeneous at ~14. A good positive correlation exists between Y and REE (R^2 = 0.98) and between Y and HREE (R^2 = 0.99). The correlation between REY and kaolinite wt.% is positive (R^2 = 0.75) except for sample L-1. A positive correlation is shown between Y and kaolinite wt.% (R^2 = 0.78) except for sample L-1. In some samples from the Caluquembe area, the REY content is >600 ppm (Table 5), which is higher than that reported in other deposits, e.g. in Uganda and Cameroon (Table 5). The size of the Caluquembe kaolin deposit (Sanematsu and Watanabe 2016) means that it can be considered as a potential non-conventional source of REY. More detailed studies are needed to determine which mineral phases are enriched in REE and the relationship between the kaolinite contents and the corresponding potential extraction of REY as a by-product during kaolinite exploitation.

CONCLUSIONS

The present work is the first study of the recently discovered kaolin deposit from the Caluquembe area (Angola).

https://doi.org/10.1007/s42860-019-00021-4 Published online by Cambridge University Press

Table 6 Mineralogical composition determined by XRPD (wt.%) of different kaolin deposits from Africa (Angola, Cameroon, Uganda, South Africa, Botswana) and worldwide (China, Czech Republic, and England).

	Caluquembe Angola whole rock granite	Mayouom western Cameroon sand-poor kaolin mylonite	Koutaba western Cameroon whole rock granite	Buwambo central Uganda whole rock granite	Migade Central Uganda whole rock granite	Mevaiela Angola <2 μm fraction anorthosite	Grahamstown South Africa Witteberg shale granite	Makoro southheastern Botswana whole rock arkose	Zhanjiang, Longyan, Guangdong province China granite	Otovice Czech Republic granite	Cornwall south-west England granite
Kaolinite	50 to 87	76 to 85	32 to 51	82 to 94	84 to 91	≈ 100	20 to 70	major	96	82 to 92	81 to 93
Quartz	0 to 23.5	2 to 9	32 to 52	0 to 10	5 to 10	detected	30 to 60	minor	0 to 1	1 to 2	1 to 2
Muscovite/illite	1 to 27	1 to 8	up to 12	3 to 6	3 to 5	detected	10 to 25	trace	3 to 4	4 to 16	4 to 15
Feldspars	2 to 21	n.d.	0 to 4	1 to 4	1 to 2	detected	5	trace	0	n.d.	n.d.
Anatase	n.d.	3.7 to 4	n.d.	n.d.	n.d.	n.d.	n.d.	n.d.	n.d.	n.d.	n.d.
Hematite/goethite	0 to 1.6	0.6 to 1.4	6 to 7	n.d.	n.d.	n.d.	n.d.	trace	n.d.	n.d.	n.d.
Pyrophilite	n.d.	n.d.	n.d.	n.d.	n.d.	n.d.	up to 35	n.d.	n.d.	n.d.	n.d.
References	This work	Njoya et al. 2006	Nkalih Mefire et al. 2015	Nyakairu et al. 2001	Nyakairu et al., 2002	Savianno et al. 2005	Heckroodt 1991	Ekosse 2000	Wilson et al. 1997	Wilson and Jiranek, 1995	Wilson and Jiranek, 1995

The kaolin samples studied do not have significant compositional or mineralogical variations. Kaolinite contents calculated from full-profile refinement by XRPD ranged between 50.4 and 87.0 wt.% and between 44.3 and 92.9 wt %, calculated using TGA (Fig. 8). The samples that crop out in shallower areas are richer in kaolinite than deeper samples. A relevant conclusion of the present work is that full-profile fitting by XRPD and TGA results have a good correlation, and the combination of both techniques is suitable for determining kaolinite contents in this type of clay deposit.

The mineralogy and compositional features of the kaolin samples indicate that Caluquembe deposits were generated by weathering of granitic rocks and the corresponding alteration of feldspars. They should, therefore, be classified as primary kaolin deposits.

The economic importance of these deposits is considered to be vital in what is an underdeveloped region. The mineralogical and compositional features of the Caluquembe kaolin and its low to medium crystallinity indicate that the most suitable application for this clay is the manufacture of structural products. Caluquembe kaolin would need to be refined and processed for use in other applications, such as in the pharmaceutical industry or in the production of paper and cosmetics.

The chondrite-normalized REE patterns show enrichment in the light REEs, the absence of a Eu anomaly, and a positive correlation has been found between kaolinite wt.% and REY content. Further studies are needed to characterize REY contents and REY carrier mineral phases. Their evaluation as a by-product in a possible future kaolinite exploitation is recommended.

ACKNOWLEDGMENTS

This research was supported by the CGL2012-36263, CGL2006-12973 and CGL2009-13758 projects of the *Ministerio de Ciencia e Innovación* of the Spanish Government, the AGAUR 2014SGR01661 project of the *Generalitat de Catalunya* and by a FI grant to J. Xu (coded FI_B 00904) sponsored by the *Secretaria d'Universitats i Recerca* of the *Departament d'Economia i Coneixement* of the *Generalitat de Catalunya*. The authors acknowledge the Scientific and Technical Centers of the University of Barcelona (CCiTUB) for their support in carrying out experimental analyses. Anonymous reviewers and the editorial staff, are thanked for helpful comments.

REFERENCES

Aagaard, P. (1974). Rare earth elements adsorption on clay minerals. *Bulletin du groupe français des argiles, **26***, 193–199.

Aparicio, P. & Galán, E. (1999). Mineralogical interference on kaolinite crystallinity index measurements. *Clays and Clay Minerals, **47***, 12–27.

Aparicio, P., Galán, E., & Ferrell, R. E. (2006). A new kaolinite order index based on XRD profile fitting. *Clay Minerals, **41***, 811–817.

Ashwal, L. D. & Twist, D. (1994). The Kunene complex, Angola/Namibia: a composite massif-type anorthosite complex. *Geological Magazine, **131***, 579–591.

Bailey, S. W. (1980). Structure of layer silicates. *Pp. 1-123 in: Crystal Structures of Clay Minerals and their X-ray Identification*. (G.W. Brindley and G. Brown, editors). Monograph, ***5***. London: Mineralogical Society.

https://doi.org/10.1007/s42860-019-00021-4 Published online by Cambridge University Press

Bao, Z., & Zhao, Z. (2008). Geochemistry of mineralization with exchangeable REY in the weathering crusts of granitic rocks in South China. *Ore Geology Reviews,* ***13***, 519–535.

Bish, D. L. (1993). Rietveld refinement of the kaolinite structure at 1.5 K. *Clays and Clay Minerals,* ***41***, 738–744.

Bermúdez-Lugo, O. (2014) *Angola and Namibia, Minerals Year Book*. U.S. Geological Survey.

De Carvalho, H., Tassinari, C., Alves, P., Guimaraes, F., & Simoes, M. C. (2000). Geochronological review of the Precambrian in western Angola: Links with Brazil. *Journal of African Earth Sciences,* ***31***, 383–402.

Detellier, C., & Schoonheydt, R. A. (2014). From platy kaolinite to nanorolls. *Elements,* ***10***, 201–206.

Dedzo, G. K. & Detellier, C. (2016). Functional nanohybrid materials derived from kaolinite. *Applied Clay Science,* ***130***, 33–39.

Dill, H. G. (2016). Kaolin: Soil, rock and ore. From the mineral to the magmatic, sedimentary and metamorphic environments. *Earth-Science Reviews,* ***161***, 16–129.

Ekosse, G.-I. (2000). The Makoro kaolin deposit, southeastern Botswana: its genesis and possible industrial applications. *Applied clay science,* ***16***, 301–320.

Ekosse, G.-I. (2010). Kaolin deposits and occurrences in Africa: Geology, mineralogy and utilization. *Applied Clay Science,* ***50***, 212–236.

Elliot, W. C., Gardner, D. J., Malla, P., & Riley, E. (2018). A new look at the occurrences of the rare-earth elements in the Georgia Kaolins. *Clays and Clay Minerals,* ***66***(3), 245–260.

Flanagan, M. D. (2016). *Clays in Mineral Commodity summaries* (Vol. **50**). U.S. Geological Survey.

Galán, E. (2006). Genesis of clay minerals, Pp, 1129–1162 in: *Handbook of Clay Science*. (F. Bergaya, B.K.G. Theng, and G. Lagaly editors) Developments in Clay Science 1. Elsevier, Amsterdam.

Galán, E., Aparicio, P., Fernández-Caliani, J.C., Miras, A., G. Márquez, M, Fallick, A. and Clauer, N. (2016) New insights on mineralogy and genesis of kaolin deposits: The Burela kaolin deposit (Northwestern Spain). *Applied Clay Science*, **131**, 14-26.

Gomes, C., Velho, J. A., & Guimaraes, F. (1994). Kaolin deposit of Mevaiela (Angola) alteration product of anorthosite: assessment of kaolin potentialities for applications in paper. *Applied Clay Science,* ***9***, 97–106.

Guggenheim, S., Adams, J. M., Bain, D. C., Bergaya, F., Brigatti, M. F., Drits, V. A., Formoso, M. L. L., Galán, E., Kogure, T., & Stanjek, H. (2006). Summary of recommendations of nomenclature committees relevant to clay mineralogy: report of the Association Internationale pour l'etude des Argiles, nomenclature committee for 2006. *Clay Minerals,* ***41***, 863–877.

Hanson, R.E. (2003). Proterozoic geochronology and tectonic evolution of southern Africa. Pp. 427–463 in: *Proterozoic East Gondwana: Supercontinent Assembly and Breakup* (M. Yoshida, B.F. Windley, and S. Dasgupta, editors). Geological Society of London, Special Publications, **206**, 427-463.

Heckroodt, R. O. (1991). Clay and clay materials in South Africa. *Journal of the South African Institute of Mining and Metallurgy,* ***91***, 343–363.

Hinckley, D. N. (1963). Variability in "crystallinity" values among the kaolin deposits of the coastal plain of Georgia and South Carolina. *Clays and Clay Minerals,* ***11***, 229–235.

Jelsma, H., Perrit, S.H., Armstrong, R.A., & Ferreira, H.F. (2011). SHRIMP U-Pb zircon geochronology of basement rocks of the Angolan Shield, western Angola. In: *Proceedings of the 23rd CAG, Johannesburg.* Council for Geoscience, Pretoria 203.

Kadir, S., & Kart, F. (2009). The occurrence and origin of the Sögüt kaolinite deposits in the Paleozoic Saricayaka granite-granodiorite complexes and overlying Neogene sediments (Bilecik, northwestern Turkey). *Clays and Clay Minerals,* ***57***, 311–329.

Laufer, F., Yariv, S., & Steinberg, M. (1984). The adsorption of quadrivalent cerium by kaolinite. *Clay Minerals,* ***19***, 137–149.

Liu, X., Liu, X., & Hu, Y. (2015). Investigation of the thermal behaviour and decomposition kinetics of kaolinite. *Clay Minerals,* ***50***, 199–209.

López-Galindo, A., Viseras, C., & Cerezo, P. (2007). Compositional, technical and safety specifications of clays to be used as pharmaceutical and cosmetic products. *Applied Clay Science,* ***36***, 51–63.

MacKenzie, R. C. (1957). *The differential thermal investigation of Clays* (456 pp). London: Mineralogical Society (Clay Minerals Group).

Mansa, R., Ngassa Piegang, G. B., & Detellier, C. (2017). Kaolinite aggregation in book-like structures from non-aqueous media. *Clays and Clay Minerals,* ***65***, 193–205.

Marques, M. M. (1977). Esboço das grandes unidades geomorfológicas de Angola (2ª aproximação). Instituto de Investigaçao Cientifica Tropical. *Garcia de Orta, Sérvicio Geologico, Lisboa,* ***2***(**1**), 41–43.

Mayer, A., Hofmann, A. W., Sinigoi, S., & Morais, E. (2004). Mesoproterozoic Sm-Nd and U-Pb ages for the Kunene Anorthosite Complex of SW Angola. *Precambrian Research,* ***133***, 187–206.

McCourt, S., Armstrong, R. A., Jelsma, H., & Mapeo, R. B. M. (2013). New U-Pb SHRIMP ages from the Lubango region, SW Angola: insights into the Palaeoproterozoic evolution of the Angolan Shield, southern Congo Craton. *Africa. Journal of the Geological Society of London,* ***170***, 353–363.

McDonough, W. F., & Sun, S. S. (1995). The composition of the earth. *Chemical Geology,* ***120***, 223–225.

Montenegro de Andrade, M. (1954). *Rochas graníticas de Angola*. Memórias, série geológica IV. Ministério do Ultramar, 464 pp.

Moore, D.M. & Reynolds, R.C. Jr. (1997). *X-Ray Diffraction and the Identification and Analysis of Clay Minerals*. Oxford University Press, 332 pp.

Murray, H. H. (1999). Applied clay mineralogy today and tomorrow. *Clay Minerals,* ***34***, 39–49.

Murray, H. H. (2000). Traditional and new applications for kaolin, smectite, palygorskite: a general overview. *Applied Clay Science,* ***17***, 207–221.

Nesbitt, H. W. & Young, G. M. (1984). Prediction of some weathering trends of plutonic and volcanic rocks based on thermodynamic and kinetic considerations. *Geochimica et Cosmochimica Acta,* ***48***, 1523–1534.

Nkalih Mefire, A., Njoya, A., Yongue Fouateu, R., Mache, J. R., Tapon, N. A., Nzeukou Nzeugang, A., Melo Chinje, U., Pilate, P., Flament, P., Siniapkine, S., Ngono, A., & Fagel, N. (2015). Occurrences of kaolin in Koutaba (west Cameroon): Mineralogical and physicochemical characterization for use in ceramic products. *Clay Minerals,* ***50***, 593–606.

Nguie, G., Dedzo, G.K. & Detellier, C. (2016). Synthesis and catalytic application of palladium nanoparticles supported on kaolinite-based nanohybrid materials. *Dalton Transactions*, 45.

Njoya, A., Nkoumbou, C., Grosbois, C., Njopwouo, D., Njoya, D., Courtin-Nomade, A., Yvon, J., & Martin, F. (2006). Genesis of Mayouom kaolin deposit (western Cameroon). *Applied Clay Science,* ***32***, 125–140.

Nyakairu, G. W. A., & Koeberl, C. (2001). Mineralogical and chemical composition and distribution of rare earth elements in clay-rich sediments from central Uganda. *Geochemical Journal,* ***35***, 13–28.

Nyakairu, G. W. A., Koeberl, C., & Kurzweil, H. (2001). The Buwambo kaolin deposit in central Uganda: Mineralogical and chemical composition. NOTE. *Geochemical Journal,* ***35***, 245–256.

Petschick, R. (2004). *MacDiff* 4.2.5. http://servermac.geologie.uni-frankfurt.de/Rainer.html.

Phipps, J. S. (2014). Engineering minerals for performance applications: an industrial perspective. *Clay Minerals,* ***49***, 1–16.

Pruett, R. J. (2016). Kaolin deposits and their uses: Northern Brazil and Georgia, USA. *Applied Clay Science,* ***131***, 3–13.

Rudnick, R.L. & Gao, R. (2003). Composition of the continental crust. Pp. 1-64 in: The Crust (R.L. Rudnick, editor). Treatise of Geochemistry, 3. Elsevier-Pergamon, Oxford, UK.

Saikia, N., Bharali, D., Sengupta, P., Bordolo, D., Goswamee, R., Saikia, P., & Borthakur, P. C. (2003). Characterization, beneficiation and utilization of a kaolinite clay from Assam, India. *Applied Clay Science,* ***24***, 93–103.

Sanematsu, K. & Watanabe, Y. (2016). Characteristics and genesis of ion adsorption-type Rare Earth Element deposits. *Reviews in Economic Geology,* ***18***, 55–79.

Savianno, G., Violo, M., Pieruccini, U., & Lopes da Silva, E. T. (2005). Kaolin deposits from the northern sector of the Cunene Anorthosite Complex (southern Angola). *Clays and Clay Minerals,* ***53***, 674–685.

Schroeder, P. A., & Erickson, G. (2014). Kaolin: From Ancient porcelains to nanocomposites. *Elements,* ***10***, 177–182.

Silva, M.V.S., (1973). Carta Geologica de Angola. Folha N 207 Gungo. Scale 1:100 000.

Silva, A.T.S.F. & Simões, M.V.C. (1980/1981). Geologia da região de Caluquembe (Angola), *Livro de Homenagem ao Professor Doutor Carlos Teixeira pela sua jubilação, Bol. Soc. Geol. Portugal*, **22**, 363–375.

Stoch, L. (1974). *Mineraly Ilaste ('Clay Minerals')* (pp. 186–193). Warsaw: Geological Publishers.

Taylor, S. R., & McLennan, S. H. (1995). The geochemical evolution of the continental crust. *Reviews of Geophysics,* ***33***, 241–265.

Thorez, J. (1975). *Phyllosilicates and clay minerals. A laboratory handbook for their X-ray diffraction analysis* (p. 580). France: Lelotte (Disno).

TOPAS (2009). *General Profile and Structure Analysis Software for Powder Diffraction Data,* version 4.2, Bruker AXS Gmbh, Karlsruhe, Germany, 2009.

Wilson, J. R., Halls, C., & Spiro, B. (1997). A comparison between the China clay deposits of China and Corwall. *Proceedings of the Ussher Society,* ***9***, 195–200.

Xiao, Y., Huang, L., Long, Z., Feng, Z., & Wang, L. (2016). Adsorption ability of rare earth elements on clay minerals and its practical performance. *Journal of Rare Earths,* ***34***(5), 543–548.

Young, R. A. & Hewat, A. W. (1988). Verification of the triclinic crystal structure of kaolinite. *Clays and Clay Minerals,* ***36***, 225–232.

(*Received 29 January 2019; revised 31 May 2019; AE: Chun-Hui Zhou*)